doi: 10.82124/CEAS-GNC-2026-039 CEAS-GNC-2026-039

Application of Gauss Pseudospectral Method to Interceptor Trajectory Design

Javier García Artieda GNC Engineer, GMV SED, Madrid, Spain. jgarcia.a@gmv.com

Miguel González Frías Senior GNC Engineer, GMV SED, Madrid, Spain. miguel.gonzalez.frias@gmv.com

Álvaro González López GNC Engineer, GMV SED, Madrid, Spain. agonzalez.l@gmv.com

Andrés Tasende Caamaño GNC Engineer, GMV SED, Madrid, Spain. atasende@gmv.com

ABSTRACT

Modern aerial threats are characterized by increasing speed, range, and manoeuvrability, presenting significant challenges for defence systems, particularly at high altitudes where low atmospheric density limits interceptor control authority. This paper addresses the interceptor trajectory design problem by formulating it as a non-linear optimal control problem solved via the Gauss Pseudospectral Method (GPM). The proposed framework utilizes a three-degree-of-freedom dynamic model. It incorporates phase-dependent aerodynamic, propulsion, and control constraints to ensure mission realism. Various configurations are investigated: single and multi-stage interceptors, the last ones equipped with double and triple-pulse propulsion systems. Numerical results demonstrate that the GPM-based approach generates feasible trajectories following an optimized ascent-descent-ascent profile. This maximizes manoeuvrability by leveraging denser atmospheric layers while complying with all constraints. A comparative analysis reveals that while triple-pulse configurations enhance high-altitude control and interception flexibility, they feature a total range reduction due to increased structural mass and lower propellant fractions. These findings confirm that GPM-based optimization is a reliable tool for planning complex interception missions. The framework shows promise for generating reference trajectories to be followed by real-time on-board guidance, improving defensive capabilities against emerging high-performance threats.

Keywords: Interceptor Trajectory, High-Altitude Interception, Gauss Pseudospectral Method, Missile Path-Planning

Nomenclature

t	=	time
c	=	chord
m	=	mass
V	=	magnitude of the velocity
γ	=	flight path angle

ξ = heading angle
T = thrust
D = aerodynamic drag
L = aerodynamic lift
Q = lateral aerodynamic force
q_∞ = dynamic pressure
S = reference surface for aerodynamics
g = gravitational acceleration
α = angle of attack
β = sideslip angle
α_c = commanded angle of attack
β_c = commanded sideslip angle
τ = first order response time constant
C_L = lift coefficient
C_D = drag coefficient
C_Q = lateral aerodynamic force coefficient
n_w = acceleration realised without gravity along velocity-w axis
$\hat{t}$ = non-dimensional time
J = cost function
ϕ = terminal cost
$\mathcal{L}$ = running cost
t_0 = initial time
t_f = final time
x = state vector
u = control vector
f = state dynamics function
C = path constraints
ψ = boundary constraints
λ = Lagrange multiplier associated with dynamic constraints
μ = Lagrange multiplier associated with path constraints
ν = Lagrange multiplier associated with boundary constraints
ℓ_i = Lagrange interpolating polynomial
D_{ki} = differentiation matrix
w_k = Gauss quadrature weights

1 Introduction

The emergence of new advanced threats generate new challenges for defence systems, because these vehicles are capable of reaching greater ranges, higher velocities, and, in some cases, significant manoeuvrability. In addition, some of them operate at very high altitudes during certain phases of flight.

A feasible countermeasure against these threats is the launch of an interceptor missile. However, this introduces a series of challenges. To provide sufficient reaction time and maximise coverage, it is desirable to have a long–range interception. This requires exploiting the full performance envelope of the interceptor. At high altitudes, the low atmospheric density reduces significantly the aerodynamic force that the interceptor can generate. This means that when the interceptor is at an altitude where it still has manoeuvring capability, it must anticipate the evolution of its future trajectory at higher altitudes and be able to plan the necessary manoeuvres while it still has the capability to perform them. Furthermore, considering that the aim is to intercept at the greatest possible distance to allow for a greater margin and that threats can fly at high speeds, the interceptor must also fly at high speed. This results in a high

relative approach velocity, which further complicates the success of the mission. It also requires more complex multi-stage or multi-pulse propulsion systems, which add further restrictions to the trajectory. Finally, it would be desirable to maintain some room for manoeuvre in order to make corrections or adapt to disturbances.

Classical guidance laws such as Proportional Navigation [1], Bias Proportional Navigation [2] and GENEX [3] are widely used and have proven their functionality and performance while requiring low computational costs. However, in these new complex scenarios, these laws fail to comply with the numerous path restrictions and boundary conditions. The inability of classical laws or guidance laws that only take into account conditions at a given moment to meet these requirements is even clearer when the point of interception is at a great distance and height. In such scenarios, it becomes even more necessary to optimise the trajectory globally. It is also necessary to take advantage of moments when there is room for manoeuvring to predict future developments and position oneself on the correct trajectory. In such cases, the use of a trajectory planner is necessary to accomplish the mission.

To obtain a trajectory that optimises the interceptor's performance and complies with all these constraints, the problem is treated in a unified manner as an optimal control problem together with all the dynamic, control, path and boundary constraints. There are two general numerical strategies for solving this optimal control problem: direct and indirect methods [4]. Indirect methods derive the conditions necessary for optimisation using Pontryagin's Minimum principle. They are very accurate, but sensitive and difficult to apply to non-linear models with strong constraints. Direct methods discretise the trajectory and transcribe the problem into a non-linear programming problem with greater robustness and easier handling of constraints, making them more suitable for this case. Among the direct techniques, pseudo-spectral methods [5, 6], in particular the Gauss Pseudospectral Method (GPM) [7], have demonstrated excellent performance in aerospace problems. It has been applied to calculate cruise missile trajectories, including complex constraints [8], or to avoid anti-aircraft defence [9], and for hypersonic cruise missile trajectories [10]. It has also been widely used for re-entry trajectories [11, 12] and for Mars landing trajectories [13].

This paper demonstrates the use of GPM as a tool for designing and optimising the trajectory of an interceptor missile while complying with realistic mission requirements and flight constraints. The document is organised as follows. Section 2 introduces the problem formulation, including the missile dynamics and main modelling aspects. Section 3 outlines the adopted methodology of the GPM. Section 4 presents and discusses the obtained trajectories under various mission scenarios, and Section 5 summarises the main findings.

2 Problem Formulation

2.1 Dynamic and Kinematic Model

The dynamic model used is based on the three degree-of-freedom aircraft performance equations in velocity axes. These dynamic equations are derived from the Euler equations of motion for a rigid body when projected in the velocity axes, the equations are well-studied so they will not be developed here [14]. The kinematic model results from integrating the velocity in Earth-fixed axes, in this case East-North-Up (ENU). The thrust is considered to be aligned with the longitudinal body axis.

Dynamics and kinematics can, therefore, be expressed in the following ODE system:

$$\frac{d}{dt}\begin{pmatrix} V \\ \gamma \\ \xi \\ x \\ y \\ z \end{pmatrix} = \begin{pmatrix} \frac{T\cos(\alpha)\cos(\beta)-D}{m} - g\sin(\gamma) \\ -\frac{n_z}{V} - \frac{g\cos(\gamma)}{V} \\ -\frac{n_y}{V\cos(\gamma)} \\ V\cos(\gamma)\cos(\xi) \\ V\cos(\gamma)\sin(\xi) \\ V\sin(\gamma) \end{pmatrix} \tag{1}$$

The simple 3 DoF equations were chosen as the optimization method is computationally intensive and this lowers the computational burden. The compromise on accuracy should be studied further, but it is usual in trajectory planning/guidance scenarios.

2.1.1 Accelerations

The accelerations considered in the previous equations include both the aerodynamic forces and the component of the thrust (aligned with x_b) projected onto the velocity axes, and they follow these expressions:

$$n_z = -\frac{T\sin(\alpha) + q_\infty S C_L}{m}; \quad n_y = -\frac{T\cos(\alpha)\sin(\beta) + q_\infty S C_Q}{m} \tag{2}$$

2.1.2 Angle of Attack and Sideslip Considerations

Even though the angle of attack and the sideslip angle are not directly involved in the dynamic model's state vector, concerning the optimization method, it is often useful to consider them part of the state vector. In this way, constraints such as limits, continuity... can be easily imposed during the different phases.

Even though in trajectory optimization problems it is common to choose the accelerations as the control variables, these are not as relevant to the problem at high altitudes as much as α and β. These angles better represent the maneuvering limitations as their maximum values vary much less during the flight, in contrast with the accelerations which depend on thrust, air density, speed... Moreover, working directly with α and β can result in lower angles for the same cumulative acceleration by leveraging low-altitude maneuvers and thrust pulses, resulting in lower control effort and a higher optimization.

Considering these observations, it is best to consider the commanded angle of attack, α_c, and commanded sideslip angle, β_c, as the control variables. It is important to make the distinction that these are the commanded angles and not the real ones, the reason for this is that a first order response is considered in the angle of attack and sideslip, which then has an effect on the other magnitudes.

$$\frac{d\alpha}{dt} = \frac{\alpha_c - \alpha}{\tau}; \quad \frac{d\beta}{dt} = \frac{\beta_c - \beta}{\tau} \tag{3}$$

This choice is made in order to model that, even though the 3 DoF model would allow instantaneous acceleration changes, a real missile has transients that need to be taken into account. Using these commands, the commanded accelerations could be computed and fed to the control system. Thus, it helps to overcome some of the difficulties that arise from using the simplified model, and if the approximation is close enough to reality, it could be used to provide control inputs for the missile with no external inputs whatsoever, no navigation inputs. It would equip the missile with "short-term resilient navigation" capabilities.

2.2 Aerodynamic Model

When using an optimizer, the simpler the aerodynamic model, the better, while still capturing the real phenomena with enough precision of course. In this case, the model chosen is detailed below:

$$C_D = C_{D_0} + C_{D_M} M + C_{D_{M^2}} M^2 + C_{D_{\alpha^2}} \alpha^2 + C_{D_{\beta^2}} \beta^2 \tag{4}$$

$$C_L = \left(C_{L\alpha} + C_{L\alpha M}\, M\right)\, \alpha \tag{5}$$

$$C_Q = \left(C_{Q\beta} + C_{Q\beta M}\, M\right)\, \beta \tag{6}$$

The coefficients for this model are calculated using a collection of semi-empirical and analytical methods [15, 16].

2.3 Missiles

There are many interceptor missiles depending on the altitude and type of threat to be intercepted. The method is shown to be suitable for different altitudes, number of stages and targets. Throughout this work, three different missiles are considered, namely:

2.3.1 Conventional Air Defense System Interceptor

A conventional air defense interceptor is usually a truck-carried surface-to-air missile (SAM). They are designed to stop threats such as aircraft, cruise missiles and tactical ballistic missiles. Our concept of a conventional interceptor is loosely based on the MIM-104 Patriot and its PAC-2/PAC-3 interceptors. Its target interception ceiling is around 20 km.

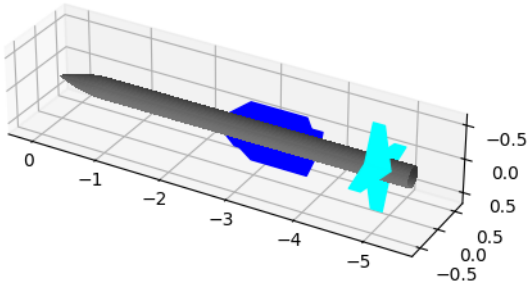

Fig. 1 Conventional Interceptor Missile

Its flight phases consist of a first pulse for take-off from the launcher, followed by a coasting phase and then a second pulse followed by coasting until impact. The second pulse can be ignited as required anytime after the first but it cannot be stopped. It is considered that this missile has no seeker.

Furthermore, the initial conditions are set to $\alpha_0 = \beta_0 = 0°$ and the final conditions are the same, assuming that the missile is hit-to-kill. The constraints on the maximum real and commanded angles are set to the same value for all phases of flight since the maximum altitude is reasonable.

$$\begin{aligned} \alpha_{min} \leq \alpha \leq \alpha_{max} \qquad & \alpha_{c\,min} \leq \alpha_c \leq \alpha_{c\,max} \quad \forall t \\ \beta_{min} \leq \beta \leq \beta_{max} \qquad & \beta_{c\,min} \leq \beta_c \leq \beta_{c\,max} \quad \forall t \end{aligned} \tag{7}$$

Naturally, continuity between phases is ensured by applying a constraint on all state variables including the aerodynamic angles on the phase transition.

2.3.2 *High Altitude Interceptor*

The second missile considered pushes the capabilities of the method further. It consists of a multiple-stage rocket for intercepting high-altitude threats.

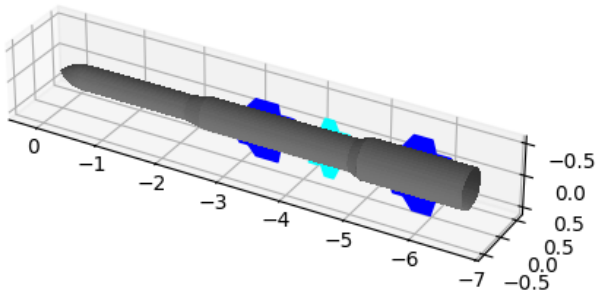

Fig. 2 High Altitude Interceptor Missile

It has three stages: boost, midcourse and terminal. After the end of each stage, it is detached and jettisoned, during which no acceleration should be commanded. Moreover, this missile makes use of a seeker, which detects, tracks and guides the missile towards its target in the final seconds of the flight. For a seeker to work correctly, it must lock on to the target. As seekers have a defined field-of-view (FOV) where they can detect the threat, the midcourse trajectory should end with the missile somewhat aligned with the target once the distance between them is close. Guidance during this stage is left to the seeker and manoeuvring is done using non-conventional controls such as DACS. It is assumed that these can generate at least enough force to maintain a straight path.

The first stage, boost, is ignited at launch. During midcourse, two options are studied:

1) **Two Pulses:** there are two propulsion pulses which can be ignited freely but once burning cannot be stopped. The flight phase sequence would consist of boost-coast-pulse-coast-pulse-coast-terminal.
2) **Three Pulses:** there are three propulsion pulses during midcourse which as before can be ignited freely but cannot be stopped. This option is reviewed in order to check if the additional higher altitude maneuverability is worth carrying that mass, in addition, the total propellant mass was considered lower due to the weight of the extra auxiliary systems. The flight phase sequence would consist of boost-coast-pulse-coast-pulse-coast-pulse-terminal.

For both cases constraints are set on the maximum values of α and β, and their commanded counterparts. Stricter limits are set on yaw movement as its demands are lower. Moreover, the maximum value is considered lower during the final coast (in two pulses) or final pulse (in three pulses) due to the inherent low maneuverability at lower densities.

Much like in the previous case, continuity between phases is ensured by applying a constraint on all state variables on each phase transition.

3 Methodology

This section presents how the Gauss pseudospectral method is applied to the calculation of the trajectory problem considered. The mathematical formulation is introduced, outlining how the continuous-time optimal control problem is transformed into a finite-dimensional nonlinear programming (NLP) problem. The pseudospectral transcription process consists of: (i) defining the optimal control prob-

lem, (ii) applying a time-domain transformation and constructing Lagrange interpolating polynomials at Legendre-Gauss points, (iii) collocating the system dynamics, and (iv) discretising the cost functional and time integration using Gauss quadrature. The resulting NLP can be solved using standard nonlinear optimisation techniques. For the interested reader, a detailed and comprehensive treatment of the Gauss pseudospectral method, along with other direct transcription approaches, can be found in [7, 17].

3.1 Optimal control problem

The path plannning problem is formulated as a Bolza-type optimal control problem over the time interval $[t_0, t_f]$:

$$J = \phi\big(x(t_f), t_f\big) + \int_{t_0}^{t_f} \mathcal{L}\big(x(t), u(t), t\big)\, dt \tag{8}$$

where $x(t) \in \mathbb{R}^{n_x}$ denotes the state vector, $u(t) \in \mathbb{R}^{n_u}$ denotes the control input, $\phi(\cdot)$ is the terminal cost, and $\mathcal{L}(\cdot)$ represents the running cost.

The system is subject to several classes of constraints. First, the state evolution is governed by the dynamic equations:

$$\dot{x}(t) = f\big(x(t), u(t), t\big) \tag{9}$$

which must be satisfied for all $t \in [t_0, t_f]$.

Second, operational, physical, or performance-related limitations are expressed through path constraints of the form:

$$C\big(x(t), u(t), t\big) \leq 0 \tag{10}$$

Finally, the problem is required to satisfy initial and terminal constraints written generally as:

$$\psi\big(x(t_0), x(t_f), t_f\big) \leq 0 \tag{11}$$

To enforce these constraints within a variational framework, an augmented cost functional is defined. Introducing the Lagrange multipliers $\lambda(t)$ associated with the dynamic constraints, $\mu(t)$ associated with the path constraints, and ν associated with the boundary constraints, the augmented functional takes the form:

$$J_a = \phi + \nu^\top \psi + \int_{t_0}^{t_f} \Big(\mathcal{L} + \lambda^\top (f - \dot{x}) + \mu^\top C\Big) dt \tag{12}$$

The objective of the following pseudospectral transcription is to convert this continuous-time optimal control problem into a finite-dimensional nonlinear programming (NLP) problem that can be solved numerically.

3.2 Time discretisation and collocation points

GPM employs Legendre-Gauss collocation nodes located strictly within the open interval $(-1, 1)$. For this reason, the original temporal domain (t_0, t_f) is mapped to the reference interval $\hat{t} \in (-1, 1)$ using the transformation:

$$t = \frac{t_f - t_0}{2}\, \hat{t} + \frac{t_f + t_0}{2} \tag{13}$$

Differentiation with respect to the new variable yields:

$$\frac{dx}{d\hat{t}} = \frac{t_f - t_0}{2}\, f\big(x(\hat{t}), u(\hat{t}), t(\hat{t})\big) \tag{14}$$

which expresses the system dynamics in the non-dimensional time.

To represent the state and control trajectories within this domain, global polynomial interpolation is employed. Let $\{\hat{t}_i\}_{i=0}^{N}$ denote a set of interpolation points in $(-1, 1)$. The state is approximated by a $N + 1$ degree Lagrange interpolating polynomial, and the control is approximated by another N degree Lagrange interpolating polynomial:

$$x(\hat{t}) \approx X(\hat{t}) = \sum_{i=0}^{N} X_i \, \ell_i(\hat{t}) \tag{15}$$

$$u(\hat{t}) \approx U(\hat{t}) = \sum_{i=1}^{N} U_i \, \ell_i^*(\hat{t}) \tag{16}$$

where $X_i(\hat{t})$ and $U_i(\hat{t})$ represent the approximation of $x(\hat{t})$ and $u(\hat{t})$ at the point $\hat{t}_i$. The i-th Lagrange polynomials $\ell_i(\hat{t})$ and $\ell_i^*(\hat{t})$ are defined as:

$$\ell_i(\hat{t}) = \prod_{\substack{j=0 \\ j \neq i}}^{N} \frac{\hat{t} - \hat{t}_j}{\hat{t}_i - \hat{t}_j}. \tag{17}$$

$$\ell_i^*(\hat{t}) = \prod_{\substack{j=1 \\ j \neq i}}^{N} \frac{\hat{t} - \hat{t}_j}{\hat{t}_i - \hat{t}_j}. \tag{18}$$

3.3 Dynamics collocation

The derivative of the interpolating polynomial at each collocation point is expressed using the pseudospectral differentiation matrix D_{ki}:

$$D_{ki} = \dot{\mathcal{L}}_i(\hat{t}_k) = \sum_{l=0}^{N} \frac{\prod_{j=0, j \neq i, l}^{N} (\hat{t}_k - \hat{t}_j)}{\prod_{j=0, j \neq i}^{N} (\hat{t}_i - \hat{t}_j)} \tag{19}$$

$$\frac{dX}{d\hat{t}}(\hat{t}_k) = \sum_{i=0}^{N} D_{ki} X_i. \tag{20}$$

Enforcing the system dynamics yields the collocation constraints:

$$\sum_{i=0}^{N} D_{ki} X_i - \frac{t_f - t_0}{2} f\left(X_k, U_k, \hat{t}_k; t_0, t_f\right) = 0 \qquad k = 1, \ldots, N. \tag{21}$$

3.4 Gauss quadrature for cost functional and time integration

Using the Gauss quadrature weights w_k, the final state value, X_f, and the cost functional, J, are approximated as

$$X_f \approx X_0 + \frac{t_f - t_0}{2} \sum_{k=1}^{N} w_k f\left(X_k, U_k, \hat{t}_k; t_0, t_f\right) \tag{22}$$

$$J \approx \phi(X_0, t_0, X_f, t_f) + \frac{t_f - t_0}{2} \sum_{k=1}^{N} w_k \mathcal{L}\left(X_k, U_k, \hat{t}_k; t_0, t_f\right) \tag{23}$$

The initial and final conditions as well as the path constraints are now expressed as:

$$\psi(X_0, t_0, X_f, t_f) = 0 \tag{24}$$

$$C(X_k, U_k, \hat{t}_k; t_0, t_f) \leq 0 \quad (k = 1, ..., N) \tag{25}$$

where path constraints are only evaluated in the discretized nodes.

3.5 Nonlinear Programming Problem

The original continuous-time optimal control problem has been converted into a finite-dimensional nonlinear programming (NLP) problem. The decision variables of the resulting NLP are given by the discrete state values $\{X_i\}_{i=0}^{N}$, the discrete control values $\{U_i\}_{i=1}^{N}$, and the final time t_f.

The resulting NLP can be written in compact form as:

$$\min_{\{X_i, U_i, t_f\}} \; \phi(X_0, t_0, X_f, t_f) + \frac{t_f - t_0}{2} \sum_{k=1}^{N} w_k \, \mathcal{L}(X_k, U_k, \hat{t}_k; t_0, t_f), \tag{26}$$

subject to:

$$\sum_{i=0}^{N} D_{ki} X_i - \frac{t_f - t_0}{2} f(X_k, U_k, \hat{t}_k; t_0, t_f) = 0, \qquad k = 1, \ldots, N, \tag{27}$$

$$\psi(X_0, t_0, X_f, t_f) = 0, \tag{28}$$

$$C(X_k, U_k, \hat{t}_k; t_0, t_f) \leq 0, \qquad k = 1, \ldots, N. \tag{29}$$

This algebraic optimisation problem is directly suitable for numerical solution using large-scale nonlinear programming solvers.

3.6 Practical implementation

The GPM transcription has been implemented following the GPOPS algorithm [18], which converts the original continuous-time optimal control problem into a finite-dimensional nonlinear programming (NLP) problem. The resulting NLP is solved using the IPOPT interior-point solver [19]. MATLAB has been used both for interfacing with the optimisation routine and for the development of custom post-processing tools to reconstruct, analyse, and export the optimised state and control trajectories.

4 Analysis and results

This section presents the numerical results obtained for three different interception scenarios. The aim is to demonstrate that the proposed tool is capable of obtaining viable trajectories that comply with the constraints and minimize the following cost function:

$$J = \int_{t_0}^{t_f} \left(\alpha^2 + \beta^2\right) dt \tag{30}$$

Three practical cases of progressive complexity are analysed. The first case is a reference scenario based on a conventional air defence interceptor. The second and third scenarios examine interceptor configurations equipped with two and three midcourse pulses and a high-altitude point of impact. This

is done to show how lower atmospheric density imposes significant limits on aerodynamic control and therefore requires careful advance planning.

4.1 First scenario

For this first scenario, the objective is to demonstrate the viability of GPM for generating the interceptor's trajectory. The interceptor presented in section 2.3.1 is used as the reference vehicle for this case. The missile is considered to be launched from the origin of the coordinate axes, with a velocity of 30 m/s, a flight path angle of 70° and a heading angle of 0°. The predicted point of impact is located at (80, 15, 20) km in the ENU reference system. The interceptor must reach this point with a flight path angle and heading angle equal to 0°, as well as its angles of attack and sideslip angle, to produce a frontal impact.

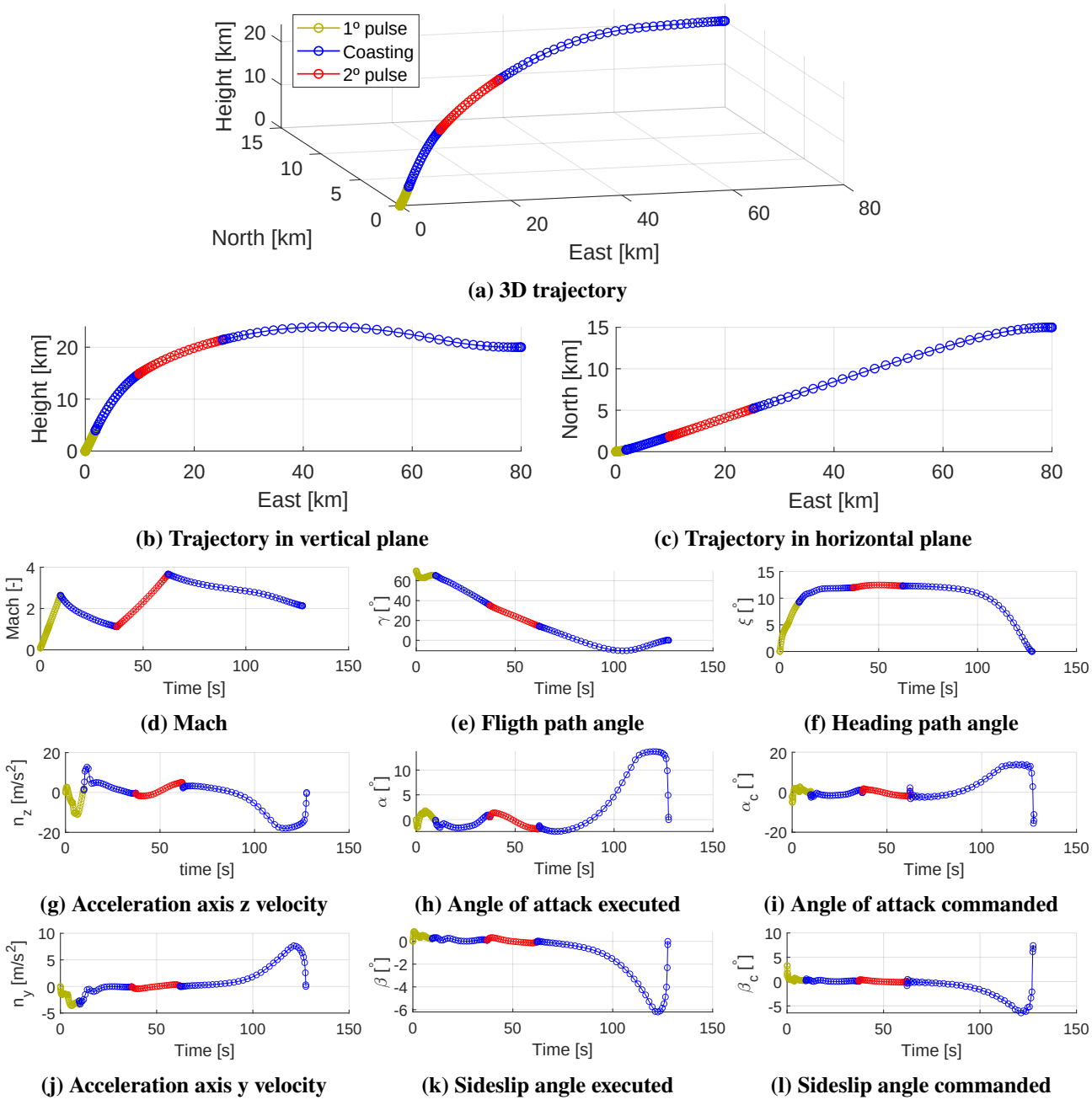

(a) 3D trajectory

(b) Trajectory in vertical plane

(c) Trajectory in horizontal plane

(d) Mach

(e) Fligth path angle

(f) Heading path angle

(g) Acceleration axis z velocity

(h) Angle of attack executed

(i) Angle of attack commanded

(j) Acceleration axis y velocity

(k) Sideslip angle executed

(l) Sideslip angle commanded

Fig. 3 Results of first scenario

For this case, the same aerodynamic angle restrictions are imposed in all phases of flight: a maximum angle of attack of 15° and a maximum lateral slip angle of 15°. In addition, the commanded angle of

attack and sideslip angle are limited to 20° to restrict the maximum rate of change of attitude angles. The start time of the second propulsion impulse is left as a free optimisation variable to allow the solver to select the most favourable ignition time.

Fig 3 presents the results obtained for the first scenario, including the evolution of the state and control variables, as well as the non-gravitational accelerations expressed in the velocity axes. The results confirm that the developed optimisation tool successfully generates a dynamically consistent trajectory that satisfies all imposed constraints.

In the vertical plane, Fig. 3b, the trajectory evolves so that gravity is the main force causing curvature during the initial segment and minimising the necessary angle of attack. In the last part, a greater angle of attack is introduced (Fig. 3h) to achieve the desired orientation at the end of the flight (Fig. 3e). With regard to the horizontal plane, during the initial stage of flight, the velocity vector is more vertical, making it easier to vary the heading angle (Fig. 3f) and requiring less acceleration. This is exploited by introducing a slight sideslip to obtain the optimal heading. Near the end of the flight, a sideslip angle is introduced (Fig. 3k) to align the vehicle with the established terminal conditions and heading.

It can be seen that, in both cases, the actual angles remain within their permitted limits, without the angle of attack or sideslip reaching saturation. Both converge to zero at the end of the trajectory as required. The actual aerodynamic angles show smooth transitions without instantaneous jumps thanks to the first-order dynamic model implemented. The commanded angles of attack (Fig. 3i) and sideslip (Fig. 3l) are also shown, which are the actual optimisation control variables.

Finally, Fig. 3g and Fig. 3j represent the accelerations that the interceptor must generate, excluding gravity. The values obtained are relatively small for a missile of this class.

4.2 Second scenario

Once the tool's ability to reproduce the dynamics of a conventional interceptor has been demonstrated, the method is used for a more demanding scenario: high-altitude interception. For this case, the interceptor model described in section 2.3.2 is used. The simulation starts at the origin with an initial velocity of 60 m/s, a heading angle of 0° and a flight path angle of 85°. The predicted point of impact is set at (190, 20, 42) km in the ENU system with 0° flight path angle and heading angle. This location has been selected because it is close to the maximum altitude and range achievable with the chosen interceptor model. The model used is equipped with a seeker, so the trajectory must reach head-on collision conditions a distance before the seeker can see the threat.

To better model changes in flight conditions, different limits are imposed on real and commanded aerodynamic angles depending on the phase. For the early phases of flight, a maximum angle of attack and a maximum sideslip of 20° are applied. During the final coasting phase, these limits are reduced to 15° for the angle of attack and 8° for the sideslip. This is done to take into account the reduced effectiveness of control at high altitude. With regard to the limits of the maximum commanded aerodynamic angles, a limit of 30° is set for the initial phases. For the final coasting phase, it is reduced to 20° following the same reasoning as before. During structural separation events at the end of the boost and at the end of the mid-course, non-gravitational accelerations are limited to zero. At the start of the seeker's acquisition phase, the vehicle must point towards the threat to ensure the seeker functions correctly. Finally, the durations of the coastings and the start times of the propulsion pulses are left as free optimisation variables.

The results for Scenario 2 are presented in Fig 4. For clarity, certain plots — such as evolution of the heading angle and the commanded aerodynamic angles — are omitted because their behaviour has already been illustrated and does not add new insight for the present analysis.

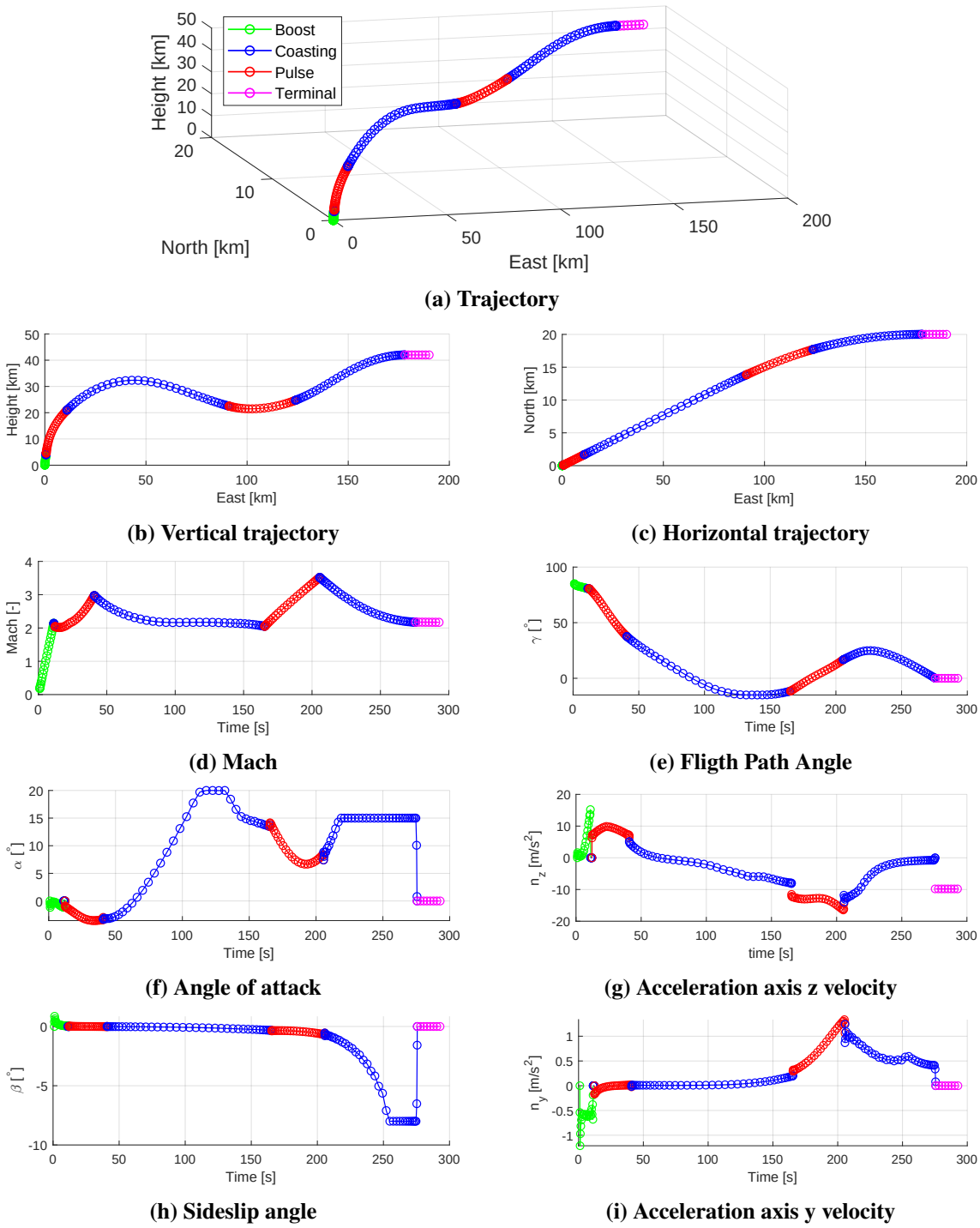

(a) Trajectory

(b) Vertical trajectory

(c) Horizontal trajectory

(d) Mach

(e) Fligth Path Angle

(f) Angle of attack

(g) Acceleration axis z velocity

(h) Sideslip angle

(i) Acceleration axis y velocity

Fig. 4 Results of second scenario

Analysing the trajectory in the vertical plane (Fig. 4b) reveals a profile that is not trivial: instead of following a simple arc directly to the PIP, the interceptor shows an ascent phase, followed by a descent and a final new ascent. This pattern is also evident in the evolution of the flight trajectory angle (Fig. 4e). The observed behaviour is due to the high distance and altitude of the PIP: the interceptor initially climbs to reduce aerodynamic drag and limit the accelerations generated on the z-axis. It then descends to an altitude where, together with a subsequent propulsion impulse, it can generate sufficient lateral authority to manoeuvre and position itself correctly before beginning the final part of the flight. This is an almost ballistic segment in which gravity mainly determines the trajectory, with little manoeuvrability, ending in the position where the seeker faces the threat with the necessary orientation. Such a complex

trajectory cannot be generated using conventional line-of-sight guidance laws, highlighting the need to use pre-planned optimisation tools to achieve viable interception solutions in these demanding conditions.

The evolution of the state and control variables is consistent with this explanation. The time evolution of γ (Fig. 4e), the angle of attack profile (Fig. 4f) and the non-gravitational acceleration on the velocity axis z (Fig. 4g) together show the sequence described above. Initially, negative α values are ordered to take advantage of gravity in the curvature of the trajectory. Subsequently, there is a saturated angle of attack at the upper limit in an attempt to delay the descent and extend the range. However, at high altitude, the missile is unable to produce enough lift to completely counter gravity, and there is a decrease in γ.

At the start of the second pulse, the combination of the thrust component orthogonal to the velocity and the lower altitude produces an increase in γ, which continues during part of the final flight while the aerodynamic lift still exceeds the weight component. This manoeuvre places the interceptor in a flight state in which the combination of speed, flight path angle, altitude and range is such that, during the final part, the vehicle can follow an almost ballistic ascent. In this final phase, although the angle of attack reaches its maximum permissible value, the aerodynamic acceleration generated is very small due to the low atmospheric density. Therefore, the vehicle must be left in such conditions beforehand to allow the trajectory to evolve naturally towards the seeker acquisition point.

On the horizontal plane (Fig. 4c, Fig. 4h and Fig. 4i), behaviour is similar to the previous case. An initial lateral acceleration is ordered, taking advantage of the high γ. As the flight progresses, the lateral slip reaches its maximum limit to align the vehicle with the theoretical threat. The corresponding lateral accelerations remain small due to the low atmospheric density.

Regarding the timing of impulse initiations, the first mid-course impulse occurs shortly after the end of the impulse phase to increase speed rapidly. The second impulse is executed at a strategic point, precisely when an increase in γ is required to initiate the final ballistic arc.

As noted above, in the terminal part of the flight, manoeuvrability is very limited due to low atmospheric density and the absence of available thrust. This limitation is intrinsic to high-altitude interception and restricts the vehicle's ability to both counter the threat's evasive manoeuvres and perform late corrective actions.

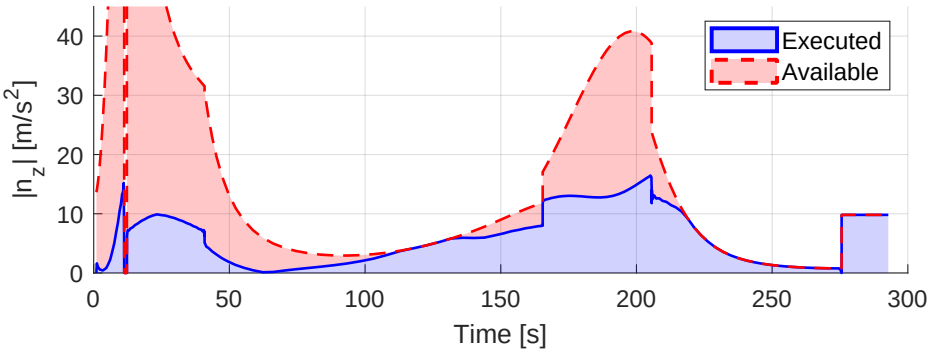

Fig. 5 Executed and maximum available acceleration along the velocity frame z-axis (absolute value) for Scenario 2

Fig 5 compares the actual non-gravitational acceleration developed by the interceptor with the maximum acceleration that could theoretically be produced. Two observations can be made from this comparison. Firstly, during a large part of the flight, the maximum acceleration available to the vehicle is already being used. This leaves little or no margin to respond to unexpected threat manoeuvres or to apply significant corrective accelerations. Second, the maximum achievable aerodynamic acceleration tends towards zero as altitude increases.

For these reasons, and to improve the interceptor's control margin during the critical transition from the midcourse to the terminal phase, dividing the midcourse phase into three pulses instead of two has been tested. This modification, discussed in the next section, is intended to allow the vehicle to have greater manoeuvrability at the end of midcourse, which is precisely where it is most needed. The following subsection presents the third scenario in detail, illustrating how the additional pulse affects the trajectory configuration and control requirements.

4.3 Third scenario

In this scenario, the intermediate trajectory segment is configured with three propulsion pulses instead of two, seeking to increase manoeuvrability near the start of the terminal phase. The initial conditions are identical to those in scenario 2, while the predicted impact point has been moved to (165, 20, 42) km in the ENU system for reasons that will be discussed later. The constraints remain virtually unchanged, with the exception of two new conditions: the last impulse must be completed before the corresponding structural separation event, and the maximum angle of attack during the final impulse has been further limited, specifically to a value of 10°. This has been done to leave sufficient margin for terminal manoeuvres.

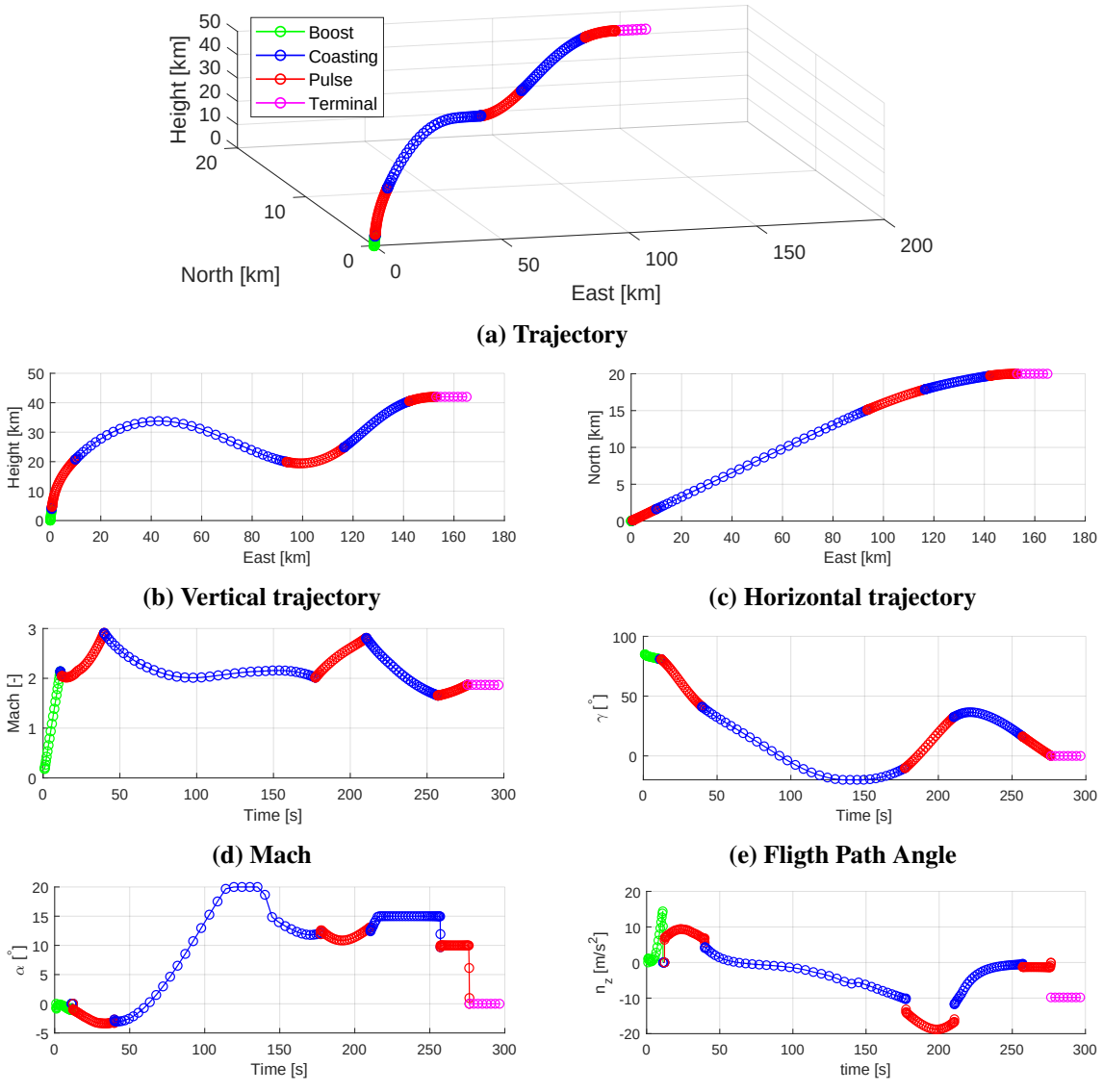

(a) Trajectory

(b) Vertical trajectory

(c) Horizontal trajectory

(d) Mach

(e) Fligth Path Angle

(f) Angle of attack

(g) Specific force axis z velocity

Fig. 6 Results of third scenario

The results of the third scenario are presented in Fig 6. The analysis focuses mainly on the vertical plane, as this provides a clearer view of the trajectory obtained by adding the additional pulse in the intermediate phase. The predicted point of impact (PIP) has moved closer to the launch point in the longitudinal direction compared to scenario 2. This is because the effective range of the interceptor is reduced in this configuration: adding an additional pulse increases the structural mass and reduces the total propellant mass. Also, the mass associated with the final pulse is carried for a longer part of the flight. As a result, the vehicle cannot reach as far as in the two-pulse configuration.

Analysing the trajectory, the general shape is qualitatively similar to that of the previous scenario, showing an initial ascent, an intermediate descent to increase the available manoeuvrability, and a final, almost ballistic ascent towards the seeker acquisition conditions. The start of the pulses shows a distribution comparable to that of scenario 2. The third pulse introduced is ignited sufficiently in advance to be completed before the structural separation event that ends the intermediate phase.

The evolution of the angle of attack (Fig. 6f) reflects the behaviour observed above: α moves towards its maximum limit during the second half of the flight in order to maximise range. Similarly, the non-gravitational acceleration on the body's z-axis (aligned with velocity) (Fig. 6g) shows a pattern similar to that in scenario 2, with the second pulse halfway through the flight providing the extra lateral acceleration needed to raise the flight path angle sufficiently.

Fig. 7 compares the actual lateral acceleration along the trajectory with the theoretical maximum available. As in scenario 2, a substantial portion of the flight utilises the vehicle's maximum available lateral acceleration, leaving little margin to counter unexpected threatening manoeuvres. However, unlike the two-pulse case, the presence of the third pulse produces a tangible, albeit modest, margin of acceleration available during the final half of the flight path. This margin is due to the terminal angle of attack limit being reduced below the aerodynamic maximum and thrust being available during the last pulse. Nevertheless, the additional acceleration margin remains small, as the component of thrust that is perpendicular to the velocity vector and with which manoeuvring is possible has a limited magnitude.

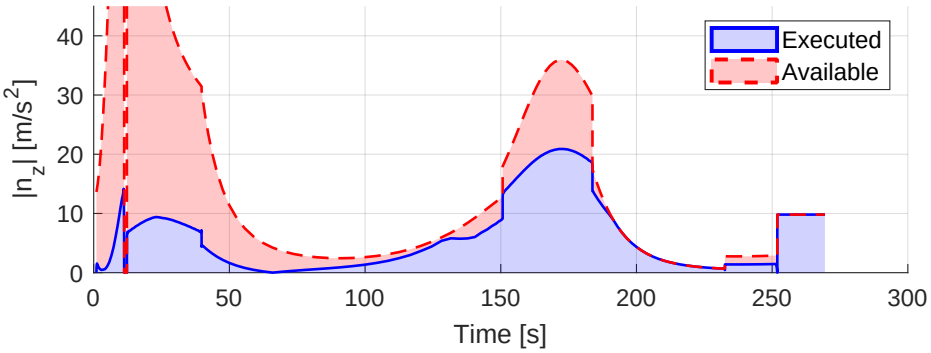

Fig. 7 Executed and maximum available acceleration along the velocity frame z-axis (absolute value) for Scenario 3

In summary, the three-pulse configuration does provide extra manoeuvring authority close to the end of midcourse, but the improvement is limited in absolute terms and comes at the cost of reduced downrange and increased system complexity.

5 Conclusions

The emergence of increasingly advanced threats places new demands on missile defence systems, especially with regard to long-range and high-altitude interceptions, where low atmospheric density limits manoeuvrability. This work has demonstrated that a trajectory planner based on the Gauss pseudospectral method can generate solutions that meet all existing constraints and limitations.

Using the GPM framework, viable interception trajectories were calculated for a series of mission scenarios. Initial tests were performed with a simpler single-stage missile model to validate the method and its numerical implementation. Next, a multi-stage interceptor with a double and triple pulse configuration in midcourse was simulated. It demonstrated the tool's ability to handle numerous coupled constraints and obtain solutions that are difficult to achieve using other tools. Comparative analysis of two-pulse versus three-pulse propulsion showed a trade-off: adding pulses can improve short-term manoeuvrability but tends to reduce the total interception range for the same mission requirements. The study also highlights the practical need to pre-plan reference trajectories to reach such extreme interception regions.

Future work will focus on enabling rapid updates or partial replanning online to adapt to changing conditions, alongside the implementation of real-time path-following algorithms to track these reference trajectories on-board.

Declaration of Use of Artificial Intelligence

During the preparation of this paper, the authors used ChatGPT to assist with improving the translation of the manuscript. All translations produced with its help were carefully reviewed and edited by the authors, who take full responsibility for the final content of the published article.

References

[1] Paul Zarchan. *Tactical and Strategic Missile Guidance, Sixth Edition*. American Institute of Aeronautics and Astronautics (AIAA), 2012. ISBN: 978-1-60086-894-8.

[2] Jang Gyu Lee Byung Soo Kim and Hyung Seok Han. Biased png law for impact with angular constraint. *IEEE Transactions on Aerospace and Electronic Systems*, 34(1):277–288, Jan. 1998. doi: 10.1109/7.640285.

[3] Ernest Ohlmeyer and Craig Phillips. Generalized vector explicit guidance. *Journal of Guidance Control and Dynamics*, 29:261–268, Mar. 2006. doi: 10.2514/1.14956.

[4] John T. Betts. Survey of numerical methods for trajectory optimization. *Journal of Guidance, Control, and Dynamics*, 21(2):193–207, May 1998. doi: 10.2514/2.4231.

[5] Divya Garg, Michael Patterson, William Hager, Anil Rao, David Benson, and Geoffrey Huntington. A unified framework for the numerical solution of optimal control problems using pseudospectral methods. *Automatica*, 46:1843–1851, Nov. 2010. doi: 10.1016/j.automatica.2010.06.048.

[6] Larry C. Young. Orthogonal collocation revisited. *Computer Methods in Applied Mechanics and Engineering*, 345:1033–1076, Mar. 2019. doi: 10.1016/j.cma.2018.10.019.

[7] David A. Benson. *A Gauss Pseudospectral Transcription for Optimal Control*. PhD thesis, Massachusetts Institute of Technology, Cambridge, MA, USA, Feb. 2005. `http://hdl.handle.net/1721.1/28919`.

[8] Timothy R. Jorris and Richard G. Cobb. Three-dimensional trajectory optimization satisfying waypoint and no-fly zone constraints. *Journal of Guidance, Control, and Dynamics*, 32(2):551–572, May 2009. doi: 10.2514/1.37030.

[9] Hu Yi and Chen Wanchun. Trajectory optimization of a cruise missile using the gauss pseudospectral method. In *The 26th Chinese Control and Decision Conference (2014 CCDC)*, pages 652–657, 2014. doi: 10.1109/CCDC.2014.6852247.

[10] Tawfiqur Rahman, Hao Zhou, Yong Sheng, Ya Younis, and Kenan Zhang. Trajectory optimization of hypersonic vehicle using gauss pseudospectral method. *Applied Mechanics and Materials*, 110-116:5232–5239, Oct. 2011. doi: 10.4028/www.scientific.net/AMM.110-116.5232.

[11] Jiang Zhao and Rui Zhou. Reentry trajectory optimization for hypersonic vehicle satisfying complex constraints. *Chinese Journal of Aeronautics*, 26:1544–1553, Dec. 2013. doi: 10.1016/j.cja.2013.10.009.

[12] Kenan Zhang and Wanchun Chen. Reentry vehicle constrained trajectory optimization. In *17th AIAA International Space Planes and Hypersonic Systems and Technologies Conference*, Apr. 2011. doi: 10.2514/6.2011-2231.

[13] Lingxia Mu, Jichi Yu, Youmin Zhang, Lidong Zhang, Guo Xie, Yuan Zhang, and Xianghong Xue. Landing trajectory generation using gauss pseudo-spectral method. In *2021 40th Chinese Control Conference (CCC)*, pages 3751–3755, July 2021. doi: 10.23919/CCC52363.2021.9550659.

[14] Bernard Etkin and Lloyd Duff Reid. *Dynamics of Flight: Stability and Control*. John Wiley & Sons, Toronto, Canada, 3 edition, 1996. ISBN: 978-0471034186.

[15] S. S. Chin. *Missile Configuration Design*. The Martin Company, Orlando, FL, USA, 1961. ISBN: 978-1019357446.

[16] F. G. Moore. *Approximate Methods for Weapon Aerodynamics*. American Institute of Aeronautics and Astronautics (AIAA), Reston, VA, USA, 2000. ISBN: 9781563473999.

[17] Geoffrey T. Huntington. *Advancement and Analysis of a Gauss Pseudospectral Transcription for Optimal Control Problems*. PhD thesis, Massachusetts Institute of Technology, Cambridge, MA, USA, June 2007. `http://hdl.handle.net/1721.1/42180`.

[18] Anil V. Rao, David A. Benson, Christopher Darby, Michael A. Patterson, Camila Francolin, Ilyssa Sanders, and Geoffrey T. Huntington. Algorithm 902: Gpops, a matlab software for solving multiple-phase optimal control problems using the gauss pseudospectral method. *ACM Trans. Math. Softw.*, 37(2), Apr. 2010. doi: 10.1145/1731022.1731032.

[19] Andreas Wächter and Lorenz Biegler. On the implementation of an interior-point filter line-search algorithm for large-scale nonlinear programming. *Mathematical programming*, 106:25–57, Apr. 2006. doi: 10.1007/s10107-004-0559-y.